European Review for Medical and Pharmacological Sciences 2023; 27: 5356-5369

DNA binding properties and cell viabilities of metal complexes derived from (*E*)-2-hydroxy-*N*′-((thiophen-2-yl)methylene)benzohydrazone and (E)-*N*′-((thiophen-2-yl)methylene) isonicotinylhydrazone

Y.-C. LIU[1], J. LUO[2], S.-Y. WANG[2], Z.-X. LIANG[2], X. ZHANG[3], B.-D. WANG[3], Y.-Y. LI[1], R.-X. LEI[1], J.-Y. WANG[1], G.-P. ZHAO[1], C.-X. BAI[1], H. CHEN[1]

[1]College of Chemistry and Chemical Engineering, FLUOBON Pilot Base of Chemical Engineering, Longdong University, Qingyang, China
[2]Qingyang Center for Disease Control and Prevention, Qingyang, China
[3]College of Chemistry and Chemical Engineering, Lanzhou University, Lanzhou, China

Abstract. – OBJECTIVE: This study aims to investigate the CT-DNA (Calf thymus DNA) binding properties and HeLa cell viabilities of metal complexes derived from (*E*)-2-hydroxy-*N'*-((thiophen-2-yl)methylene)benzohydrazone (H_2L^1) and (*E*)-*N'*-((thiophen-2-yl)methylene)isonicotinylhydrazone (HL^2).

MATERIALS AND METHODS: A series of metal complexes derived from (*E*)-2-hydroxy-*N'*-((thiophen-2-yl)methylene)benzohydrazone (H_2L^1) and (*E*)-*N'*-((thiophen-2-yl)methylene)isonicotinylhydrazonewere (HL^2) were synthesized, and their structures were characterized through FT-IR, ESI-MS, elemental analysis, molar conductivities and X-ray diffraction. DNA binding properties between CT-DNA and metal complexes were investigated by UV-Vis spectrophotometry and viscosity titration. The toxicological properties of compounds on HeLa cell were measured *in vitro*.

RESULTS: Ligand H_2L^1 or HL^2 exhibits a tridentate and anion ligand and uses oxygen anion, nitrogen atom and sulfur atom to coordinate with metal ions. When coordinated with metal ions, the unit O=C–NH– of each ligand has been enolized and deprotonated into –O–C=N–. The suggested chemical formulas of metal complexes are: $[Co(HL^1)_2]$, $[Ni(HL^1)_2]$, $[Cu(HL^1)_2]$, $[Co(L^2)_2]$, $[Cu(L^2)_2]$, $[Zn(L^2)_2]$, $[ScL^2(NO_3)_2(H_2O)_2]$, $[Pr(L^2)_2(NO_3)]$ and $[Dy(L^2)_2(NO_3)]$. Both ligands and their metal complexes can bind strongly to CT-DNA through hydrogen bond and intercalation with K_b of 10^4~10^5 L mol^{-1} compared to ethidium bromide [classical DNA intercalator, $K_{b(EB-DNA)} = 3.068 \times 10^4$ L mol^{-1}]; however, the groove pattern cannot be excluded. The coexistence of multiple binding modes may be a common form of drug binding to DNA. HeLa cell shows lower viabilities in the presence of $[Ni(HL^1)_2]$ and $[Cu(HL^1)_2]$ ($^*p < 0.05$) compared to the other compounds, with the LC_{50} of 2.6 μmol L^{-1} and 2.2 μmol L^{-1}, respectively.

CONCLUSIONS: These compounds, especially $[Ni(HL^1)_2]$ and $[Cu(HL^1)_2]$, will be promising for anti-tumor drugs, which should be further studied.

Key Words:
Metal complex, DNA binding property, DNA binding mode, Intercalation, Cell viability.

Introduction

The heterocyclic compounds containing sulfur are the most promising substances in drug development today. Benzothiophene derivatives have been used for anti-allergy, analgesia, anti-inflammatory, ocular hypotension and osteoporosis related to postmenopausal women[1-5]. Isoniazid is one of first-line anti-tuberculosis drugs commonly used in clinic. However, due to the long course of treatment, patients may have drug resistance because of the interruption of treatment. After isoniazid resistance, the re-sensitization rate of 88.5% could be achieved after 36 weeks of drug withdrawal. The occurrence of drug resistance is also related to the gene mutation of *Mycobacterium tuberculosis* (MTB)[6,7]. The oxazolidinone drug linezolid is mainly used for severe infections caused by multidrug-resistant Gram-positive bacteria. However, emerging linezolid resistance is aggravating difficulties in the treatment of certain infectious diseases. *OptrA* discovered is a gene

Corresponding Author: Yong-Chun Liu, Ph.D; e-mail: ychliu001@163.com

encoding oxazolidinone resistance, which exists in both plasmids and chromosomes, but mostly plasmids. The emergence of the novel plasmid-borne ABC transporter gene *optrA* expanded the understanding of the mechanism of linezolid resistance[8]. Liu and Zhao[9] found that miR-217 can silence the expression of CUL4B, inhibit the activation of Wnt/β-catenin signaling pathway, enhance the cisplatin sensitivity and reverse drug resistance, inhibit cell invasion and migration, and promote cell apoptosis. The enhancement of multidrug resistance (MDR) encourages researchers to look for new metal complexes as new antibacterial agents[10]. Lanthanide complexes have been studied as inhibitors and cytotoxic agents in photodynamic therapy, radiotherapy, drug delivery, biosensors, bioimaging, anti-tumor and antithrombotic agents[11-13]. Additionally, hydrazide compounds have been found to have high reaction performance and wide application. They have many coordination atoms, such as oxygen and nitrogen, which can then react and coordinate with metal ions to form metal chelates with stable and special structures[14]. Moreover, compounds derived from Schiff base have also shown good antitumor activities against animal tumors[15,16]. On the other hand, many chemicals play an anti-tumor role by combining with DNA, and its effectiveness depends on the way of combination and affinity[17-19]. Many metal chelates are used as mediators and chemotherapeutic agents for double stranded DNA fragmentation, and as probes for DNA structure in solution[20-22].

Previously, complexes prepared from (*E*)-2-hydroxy-N'-((thiophen-2-yl)methylene)benzohydrazone and La^{3+}, Sm^{3+}, Eu^{3+}, Dy^{3+} ions presented better antibacterial and antifungal activities *in vitro*[8]. Complexes prepared from (*E*)-2-hydroxy-N'-((thiophen-2-yl)methylene)benzohydrazone and Zn^{2+}, Cu^{2+}, Ni^{2+}, Co^{2+} ions also presented antimicrobial activities[23]. In this research, a series of metal complexes derived from (*E*)-2-hydroxy-N'-((thiophen-2-yl)methylene)benzohydrazone and (*E*)-N'-((thiophen-2-yl)methylene)isonicotinylhydrazone were synthesized, then the CT-DNA interacting properties and HeLa cell viabilities were studied.

Materials and Methods

Materials

Both of Calf thymus DNA and Ethidium bromide (EB) were purchased from Sigma-Aldrich Biotech. Co., Ltd. (Sigma-Aldrich, St. Louis, MO, USA), and they were dissolved individually in buffer solution of 5 mmol L^{-1} Tris-HCl containing 50 mmol L^{-1} NaCl with pH 7.20. The concentration of CT-DNA in terms of nucleotide^{-1} and base pair L^{-1} was determined as literature[24], and the concentration of EB was also determined as literature[25]. 2-Thiophenecarbaldehyde was purchased from J&K Scientific Chemical Reagent Company. Both ligands and complexes were dissolved individually in dimethyl sulfoxide (DMSO) for further investigation.

Methods

Both ligands (*E*)-2-hydroxy-*N'*-((thiophen-2-yl)methylene)benzohydrazone (H_2L^1) and (*E*)-*N'*-((thiophen-2-yl)methylene)isonicotinylhydrazone (HL^2) were synthesized on two steps referring to the literatures[8,23], as shown in Figure 1, respectively. The metal complexes were prepared through refluxing equimolar amounts of $Cu(NO_3)_2{\cdot}6H_2O$, $Ni(NO_3)_2{\cdot}6H_2O$, $Co(NO_3)_2{\cdot}6H_2O$ and H_2L^1 (0.2 mmol, 0.049 g) in a 30 ml of methanol solution, respectively. After refluxing for 30

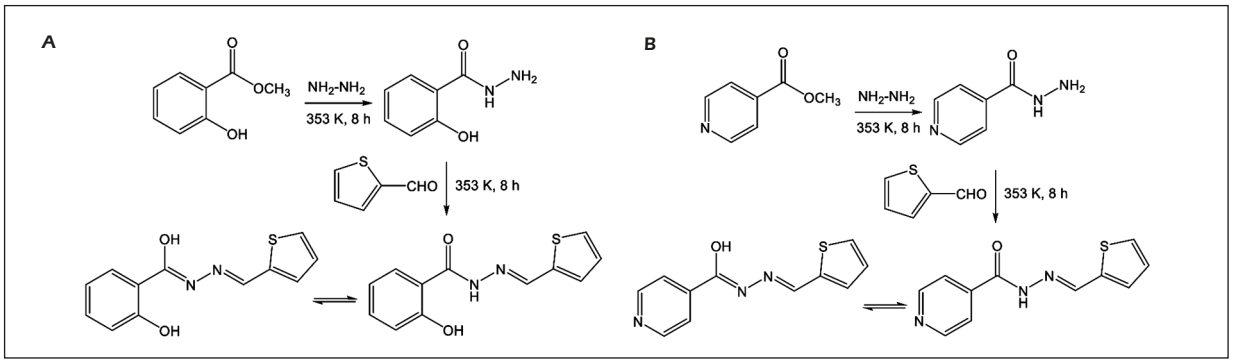

Figure 1. The synthetic routes of ligands H_2L^1 (**A**) and HL_2 (**B**).

minutes, 2-3 drops of triethylamine were added to the reaction system. After 8 hours, the mixture was centrifugated and washed with methanol, and then dried in vacuum for 48 hours, besides the precipitate of Sc^{3+} complex was gained by vapor diffusion. The metal complexes derived from HL^2 and $Co(NO_3)_2 \cdot 6H_2O$, $Cu(NO_3)_2 \cdot 6H_2O$, $Zn(NO_3)_2 \cdot 6H_2O$, $Sc(NO_3)_3 \cdot 6H_2O$, $Pr(NO_3)_3 \cdot 6H_2O$ and $Dy(NO_3)_3 \cdot 6H_2O$ were prepared as the same procedures for H_2L^1, where the amount of HL^2 was taken as 0.2 mmol (0.046 g).

The FT-IR spectra (Nicolet Nexus 670), ESI-MS (ESI-Trap/Mass, Bruker Esquire 6000), X-ray diffraction (Bruker APEX area-detector diffractometer), elemental analyses and molar conductance were used to characterize the structures of the investigated compounds.

The viscosity titration experiment[24-26] and UV-Vis titration spectra (Specord 50, Analytik Jena, Jena, Germany) were used to determine the interaction modes and abilities between the investigated compounds and CT-DNA. The binding constant (K_b) was calculated as the following equation[27,28]:

$$\frac{[DNA]}{\varepsilon_f - \varepsilon_a} = \frac{[DNA]}{\varepsilon_f - \varepsilon_b} + \frac{1}{K_b(\varepsilon_f - \varepsilon_b)} \quad (1)$$

[DNA] represents molar concentration of CT-DNA in base pair; ε_a, ε_f and ε_b correspond to the observed extinction coefficient, extinction rate of free compound, and extinction efficiency when the compound is completely combined with CT-DNA.

UV-Vis spectra were also used to study the replacement of EB by present compound in DNA-EB system. 112 µl DNA of 1.0 µmol L^{-1} (nucleotides) were added into a 2.5 ml of 10.0 µmol L^{-1} solution of EB to obtain a DNA-EB system (C_{DNA}:C_{EB} = 4.5:1), where DNA and EB interacted and reached to saturation[29]. Then to the above system, 25 µl present compound solution of 1.0 mmol L^{-1} were added each time till 250 µl. The time interval of each addition of investigated compound into CT-DNA system was controlled within 5 minutes, both in viscosity titration and UV-Vis titration experiments.

The cell compatibility of materials was confirmed by using Hela cells. Hela cells were seeded in 96-well plate (1×10^4 cells per well) beforehand. After 24 h incubation, cells were washed by PBS. Fresh cell culture medium contained different concentrations of materials (0, 0.4, 0.6, 0.8, 1, 2, 4, 6, 8, 10, 20, 40 and 60 µmol L^{-1}). After a 24-hours incubation, 100 µl fresh culture medium containing 10% CCK-8 was added. The absorbance that represented the cell viability was measured by a microplate reader at the wavelength of 450 nm[30].

Statistical Analysis

Each experiment of cell viability assay was conducted three times in parallel, and the relative data were expressed as the mean ± standard error of the mean. Additionally, the statistical significance difference was shown as $*p < 0.05$, $**p < 0.01$, and $***p < 0.001$. The cell viability ratio of HeLa *vs.* concentration of compound was calculated as the following equation:

$$\textit{The cell viability ratio} = \frac{A_s}{A_b} \quad (2)$$

A_s and A_b represent the absorbance measured by a microplate reader at the wavelength of 450 nm in the presence and in the absence of samples investigated, respectively.

LC_{50} (half lethal concentration) was calculated by fitting mathematical formula with scatter plot of cell viability ratio of HeLa at 0.50 *vs.* concentration of compound.

Results

Syntheses of Ligands H_2L^1 and HL^2 and Their Metal Complexes

The basic data of compounds including chemical formula, yield, melting point, color, ESI-MS (m/z^+), IR (KBr) and Λm (DMSO) were listed as below:

H_2L^1: $C_{12}H_{10}N_2O_2S$. Yield: 64.5%. M.p. = 246°C. Pale yellow. ESI-MS (m/z^+): 247.1128 $[M+H]^+$ (dimethyl sulfoxide, DMSO). IR (KBr): 3441, 3223, 1676, 1593, 1526, 845 cm^{-1}. Λm (DMSO) = 3.7 cm^2 Ohm^{-1} mol^{-1}.

HL^2: $C_{11}H_9N_3O_2S$. Yield: 52.5%. M.p. = 234°C. Pale yellow. ESI-MS (m/z^+): 232.1129 $[M+H]^+$ (DMSO). IR (KBr): 3207, 1678, 1576, 1510, 849 cm^{-1}. Λm (DMSO) = 1.7 cm^2 Ohm^{-1} mol^{-1}.

$[Co(HL^1)_2]$: Yield: 66.4%. Brown. M.p. ≥ 300°C. Anal. calcd. for $C_{24}H_{18}CoN_4O_4S_2$. C 52.46, H 3.30, Co 10.73, N 10.20, O 11.65, S 11.67; found: C 52.55, H 3.22, Co 10.80, N 10.36,

O 11.71, S 11.56. ESI-MS (m/z^+): 549.1126 $[M]^+$ (DMSO). IR (KBr): 3447, 1622, 1558, 1508, 756, 579, 534, 457, 438 cm^{-1}. Λm (DMSO) = 5.7 cm^2 Ohm^{-1} mol^{-1}.

$[Ni(HL^1)_2]$: Yield: 65.2%. Orange. M.p. ≥ 300°C. Anal. calcd. for $C_{24}H_{18}NiN_4O_4S_2$. C 52.48, H 3.30, N 10.20, Ni 10.69, O 11.65, S 11.67, found: C 52.40, H 3.21, N 10.37, Ni 10.76, O 11.51, S 11.52. ESI-MS (m/z^+): 549.0938 $[M]^+$ (DMSO). IR (KBr): 3420, 1622, 1582, 1516, 752, 534, 478, 419 cm^{-1}. Λm (DMSO) = 10.5 cm^2 Ohm^{-1} mol^{-1}.

$[Cu(HL^1)_2]$: Yield: 63.4%. Green. M.p. ≥ 300°C. Anal. calcd. for $C_{24}H_{18}CuN_4O_4S_2$. C 52.02, H 3.27, Cu 11.47, N 10.11, O 11.55, S 11.57; found: C 52.13, H 3.15, Cu 11.40, N 10.06, O 11.49, S 11.70. ESI-MS (m/z^+): 554.0100 $[M]^+$ (DMSO). IR (KBr): 3447, 1622, 1587, 1508, 785, 536, 474, 420 cm^{-1}. Λm (DMSO) = 12.0 cm^2 Ohm^{-1} mol^{-1}.

$[Co(L^2)_2]$: Yield: 62.8%. Brown. M.p. ≥ 300°C. Anal. calcd. for $C_{22}H_{16}CoN_6O_2S_2$. C 50.87, H 3.10, Co 11.35, N 16.18, O 6.16, S 12.34; found: C 50.77, H 3.19, Co 11.28, N 16.27, O 6.05, S 12.21. ESI-MS (m/z^+): 519.1040 $[M]^+$ (DMSO). IR (KBr): 1589, 1514, 775, 575, 519, 442, 419 cm^{-1}. Λm (DMSO) = 20.0 cm^2 Ohm^{-1} mol^{-1}.

$[Cu(L^2)_2]$: Yield: 63.2%. Green. M.p. ≥ 300°C. Anal. calcd. for $C_{22}H_{16}CuN_6O_2S_2$. C 52.42, H 3.08, Cu 12.13, N 16.04, O 6.11, S 12.23; found: C 52.33, H 3.17, Cu 12.25, N 16.11, O 6.27, S 12.35. ESI-MS (m/z^+): 524.1052 $[M]^+$ (DMSO). IR (KBr): 1568, 1501, 781, 569, 519, 457, 419 cm^{-1}. Λm (DMSO) = 13.0 cm^2 Ohm^{-1} mol^{-1}.

$[Zn(L^2)_2]$: Yield: 66.4%. Yellow. M.p. ≥ 300°C. Anal. calcd. for $C_{22}H_{16}ZnN_6O_2S_2$. C 50.24, H 3.07, N 15.98, O 6.08, S 12.19, Zn 12.43; found: C 50.15, H 3.16, N 15.84, O 6.11, S 12.26, Zn 12.35. ESI-MS (m/z^+): 396.4267 $[M+H]^+$ (DMSO). IR (KBr): 1616, 1568, 1506, 777, 555, 474 cm^{-1}. Λm (DMSO) = 15.0 cm^2 Ohm^{-1} mol^{-1}.

$[ScL^2(NO_3)_2(H_2O)_2]$: Yield: 48.1%. Yellow. M.p. ≥ 300°C. Anal. calcd. for $C_{11}H_{12}N_5O_9SSc$. C 30.35, H 2.78, N 16.09, O 33.08, S 7.37, Sc 10.33; found: C 30.48, H 2.87, N 16.13, O 33.21, S 7.40, Sc 10.20. ESI-MS (m/z^+): 437.2804 $[M+H]^+$ (DMSO). IR (KBr): 3234, 1589, 1514, 1242, 1045, 941ρ_r, 775, 656ρ_w, 579, 530, 467 cm^{-1}. Λm (DMSO) = 6.8 cm^2 Ohm^{-1} mol^{-1}.

$[Pr(L^2)_2(NO_3)]$: Yield: 59.1%. Yellow. M.p. ≥ 300°C. Anal. calcd. for $C_{25}H_{16}N_7O_5PrS_2$. C 45.26, H 2.43, N 14.78, O 12.06, S 9.66, Pr 21.24; found: C 45.10, H 2.34, N 14.82, O 12.11, S 9.78, Pr 21.30. ESI-MS (m/z^+): 685.4227 $[M+Na]^+$ (DMSO). IR (KBr): 1589, 1516, 1242, 1057, 771, 559, 536, 474, 446 cm^{-1}. Λm (DMSO) = 6.8 cm^2 Ohm^{-1} mol^{-1}.

$[Dy(L^2)_2(NO_3)]$: Yield: 57.1%. Pale yellow. M.p. ≥ 300°C. Anal. calcd. for $C_{25}H_{16}DyN_7O_5S_2$. C 38.57, H 2.35, N 14.31, O 11.68, S 9.36, Dy 23.72; found: C 38.42, H 2.26, N 14.44, O 11.55, S 9.48, Dy 23.60. ESI-MS (m/z^+): 685.4200 $[M]^+$ (DMSO). IR (KBr): 1583, 1524, 1238, 1055, 773, 608, 473, 419 cm^{-1}. Λm (DMSO) = 22.6 cm^2 Ohm^{-1} mol^{-1}.

Viscosity Titration Experiment

The effects of viscosity $(\eta/\eta_o)^{1/3}$ *vs.* $C_{compound}/C_{DNA\ (bps)}$ are shown in Figure 2, where the concentration of CT-DNA is 50 µmol L^{-1} as base pairs.

UV-Vis Titration Experiment

The UV-Vis overlapped spectra of HL^2 and its complex $[Co(L^2)_2]$ with successive addition of CT-DNA (4.0-40.0 µmol L^{-1}) are shown in Figure 3.

The UV-Vis overlapped spectra of EB+DNA+HL^2 (a) and EB+DNA+$[Co(HL^2)_2]$ (b) are shown in Figure 4.

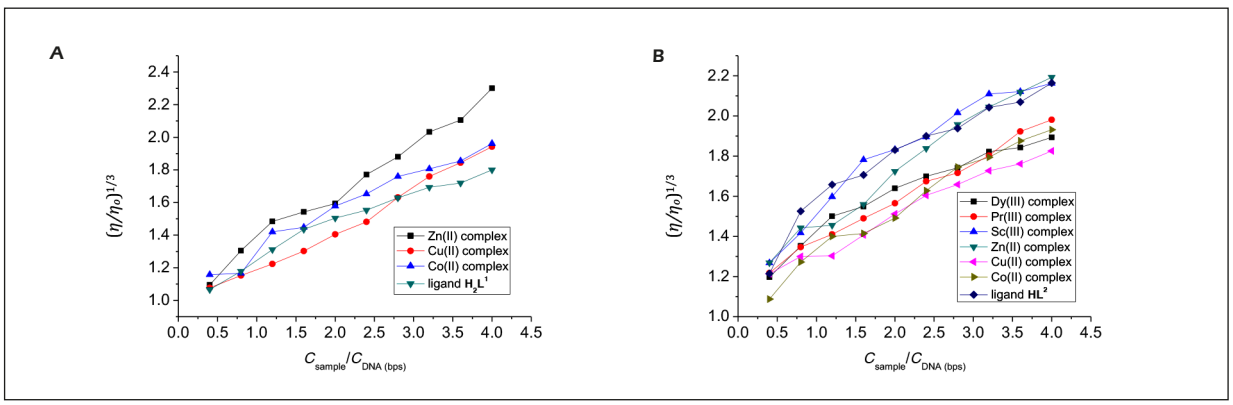

Figure 2. The effects of viscosity $(\eta/\eta_o)^{1/3}$ *vs.* $C_{compound}/C_{DNA\ (bps)}$. The concentration of CT-DNA was 50 µmol L^{-1} as base pairs. **A**, Ligand H_2L^1 and its complexes and CT-DNA systems. **B**, ligand HL^2 and its complexes and CT-DNA systems.

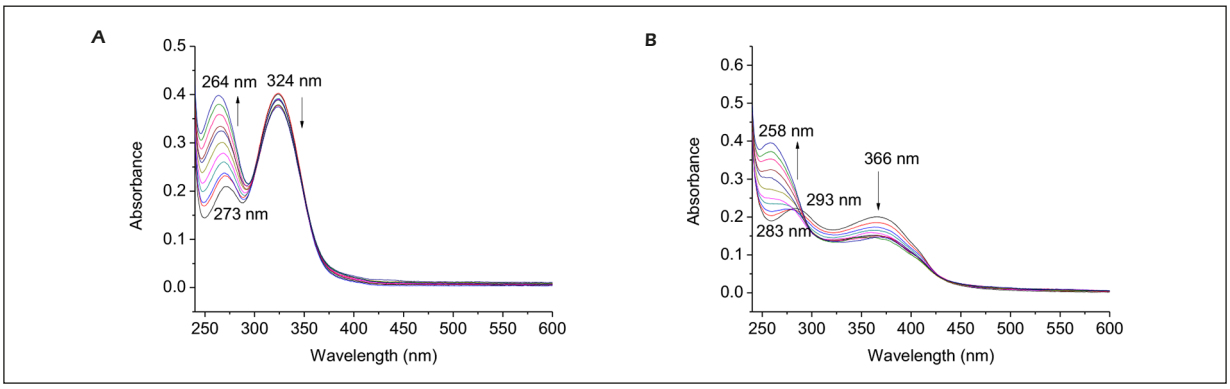

Figure 3. The UV-Vis overlapped spectra of ligand HL^2 (**A**) and its complex $[Co(HL^2)_2]$ (**B**) with successive addition of CT-DNA (4.0-40.0 μmol L^{-1}), respectively.

Cell Viability Assay

The cell viability and cell viability ratio (100% control) of HeLa cells *vs.* concentration of ligand H_2L^1 and its complexes $[Ni(HL^1)_2]$ and $[Cu(HL^1)_2]$ *in vitro* are listed in Table I (all the statistical significance $*p < 0.05$; other data are not listed), and the plot of cell viability ratios (100% control) of HeLa cells *vs.* concentration of ligands (a) and their complexes (b) are shown in Figure 5.

Discussion

Characteristics of Ligands H_2L^1 and HL^2 and Their Metal Complexes

Both of the ligands H_2L^1 and HL^2 are pale yellow and stable in air, and the melting points are 246°C and 234°C, respectively. FT-IR spectra (KBr; ν_{max}, cm^{-1}) of H_2L^2 show bands of 3,441 s, 3,223, 1,676, 1,593, 1,526 and 845, belonging to ν (OH), ν (NH), ν (C=O), ν (C=N), ν (C=N, enolic) and ν (C–S), respectively. On the other hand, FT-IR spectra (KBr; ν_{max}, cm^{-1}) of HL^2 show bands of 3,207, 1,678w, 1,576, 1,510 and 849, belonging to ν (NH), ν (C=O), ν (C=N, pyridine), ν (C=N, enolic) and ν (C–S), respectively. The pale-yellow transparent crystal of ligand HL^2 was gained by vapor diffusion for 3 days. X-ray structural calculation was carried out through the programs SHELXS-97 and SHELXL-97[31]. X-ray crystal structure of HL^2 shows its crystal system and space group are monoclinic *Cc*, as listed in Table II. The supporting material for crystal structure of HL^2 has been deposited with the CCDC No. 2169641. The comparison of measured bond length of ligand HL^2 with normal bond length is listed in Table III. The measured bond length of C–N [1.337(4) Å] of unit HO–C=NH– is shorter than the normal C-N (1.47-1.50 Å) and squared with C=N (conjugate), and C–O [1.218(4) Å] shortens but still maintains the normal characteristics of (C···)C=O (1.19-1.23 Å)[32].

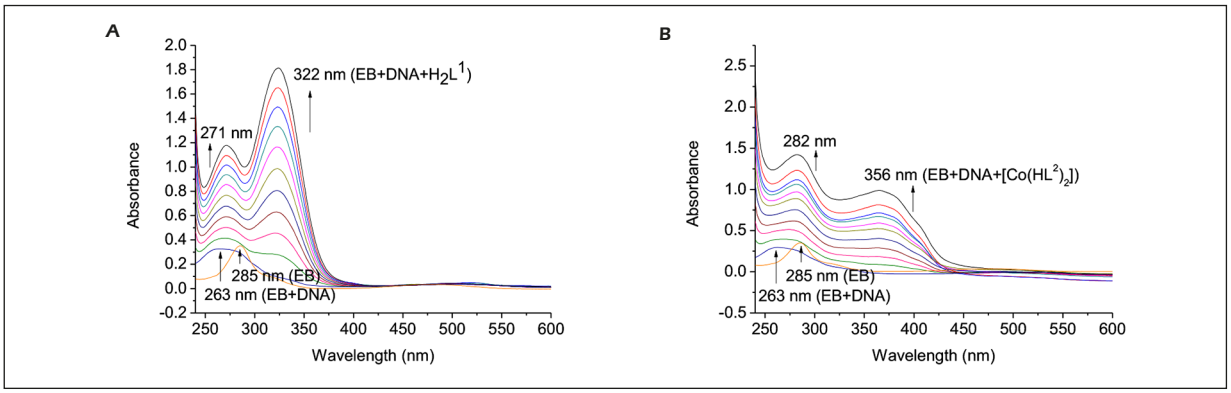

Figure 4. The UV-Vis overlapped spectra of EB+DNA+HL^2 system (**A**) and EB+DNA+$[Co(HL^2)_2]$ system (**B**), respectively.

Table I. Data of cell viability (100% control) of HeLa cells *vs.* concentration of ligand H_2L^1 and its complexes $[Ni(HL_1)^2]$ and $[Cu(HL^1)_2]$.

	H_2L^1		$[Ni(HL^1)_2]$		$[Cu(HL^1)_2]$	
C (μmol L^{-1})	Cell viability	Cell viability ratio	Cell viability	Cell viability ratio	Cell viability	Cell viability ratio
0	0.7387 ± 0.1114	1.00	1.3521 ± 0.0282	1.00	1.4819 ± 0.1712	1.00
0.4	–	–	1.2597 ± 0.1095	0.9317	1.4424 ± 0.1964	0.9733
0.6	–	–	1.2204 ± 0.0228	0.9026	1.3255 ± 0.0983	0.8945
0.8	–	–	1.1530 ± 0.1018	0.8527	1.0050 ± 0.2150	0.6782
1.0	–	–	0.8548 ± 0.1156	0.6322	0.7394 ± 0.0783	0.4990
2.0	–	–	0.6056 ± 0.0979	0.4479	0.8210 ± 0.2462	0.5540
4.0	0.4393 ± 0.0425	0.5947	0.3200 ± 0.0355	0.2367	0.5152 ± 0.1037	0.3477
6.0	0.5971 ± 0.0461	0.8083	0.2979 ± 0.1151	0.2203	0.2493 ± 0.0172	0.1682
8.0	0.7278 ± 0.0954	0.9852	0.2840 ± 0.0648	0.2100	0.3947 ± 0.1102	0.2663
10.0	0.6305 ± 0.0825	0.8535	–		–	
20.0	0.6699 ± 0.0808	0.9069	–		–	
40.0	0.6525 ± 0.0278	0.8833	–		–	
60.0	0.3638 ± 0.0189	0.4925	–		–	
p	0.012		0.00004		0.002	

The standard errors for cell viability ratio that are not listed are as the same as those for cell viability.

This indicates that the unit O=C–NH– has enolized partly into the unit of HO–C=N–, resulting in a larger conjugate system of HL^2.

All of the complexes derived from ligand H_2L^1 are stable, soluble in DMSO, non-electrolytes[33] with molar conductivities of 5.7-12.0 cm^2 Ohm^{-1} mol^{-1}, and their melting points exceed 300°C. Carefully compared with the FI-IR spectra of ligand H_2L^1, the broad and strong bands of phenolic OH (3,420-3,447 cm^{-1}) for all the present complexes indicate they are not involved in coordination. The bands of N–H of 3,223 cm^{-1} disappear, and new bands of 1,622 cm^{-1} and 1,516-1,508 cm^{-1} appear, indicating that the unit O=C–NH– has enolized and deprotonated into the unit of $^-$O–C=N–, and O^- and N of $^-$O–C=N– involves in coordination. Additionally, the new bands of 785-752 cm^{-1}, 579-534 cm^{-1} and 478-419 cm^{-1} show further formations of M–S, M–O and M–N bonds, respectively. Combined with molar conductivities, elemental analysis, FT-IR and ESI-MS (m/z^+), it suggests that H_2L^1 exhibits a tridentate and anion ligand and uses oxygen anion, nitrogen atom and sulfur atom to coordinate with metal ions of Cu^{2+}, Ni^{2+} and Co^{2+}. Their suggested chemical structures are presented in Figure 6a, which is almost consistent with the structures reported in the literature[23].

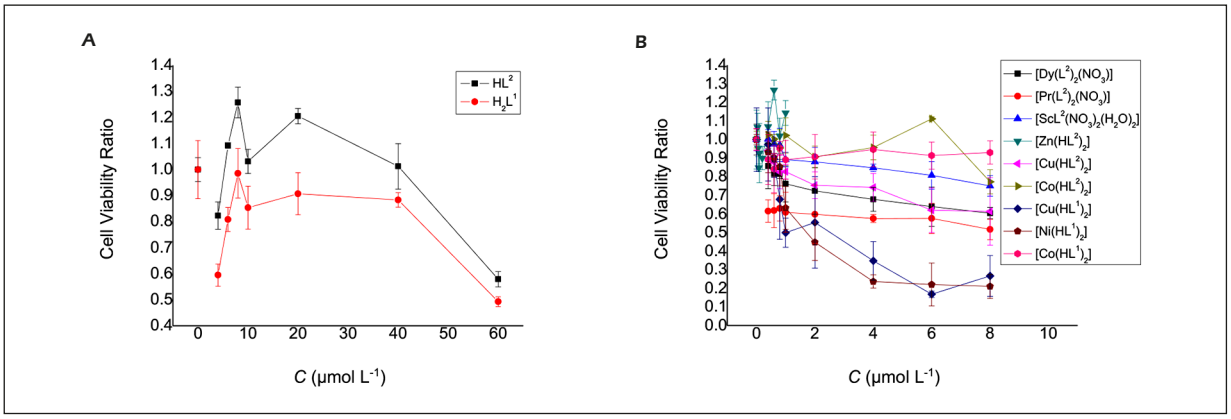

Figure 5. The cell viability ratio (100% control) of HeLa *vs.* concentration of ligands (**A**) and their complexes (**B**).

Table II. Crystal structure refinement of ligand HL^2.

Compound	HL^2
Chemical formula	$C_{11}H_9N_3OS$
Formula weight	231.27
T (K)	298(2)
Wavelength (Å)	0.71073
Radiation	Mo Kα
Crystal system	Monoclinic
Space group	*Cc*
a (Å)	10.0143(13)
b (Å)	13.6167(14)
c (Å)	8.5459(11)
α (°)	90.000
β (°)	111.668(4)
γ (°)	90.000
V (Å^3)	1083.0(2)
Z	4
Dc (g cm^{-3})	1.418
μ (mm^{-1})	0.279
F (000)	480
Crystal size (mm)	0.45×0.28×0.24
$\theta_{min/max}$ (°)	2.65–25.02
Index ranges	$-11 \le h \le 11$, $-16 \le k \le 16$, $-9 \le l \le 10$
Reflections collected/ unique	2,535/1,435 [$R_{(int)} = 0.0393$]
Completeness to theta = 25.02	99.3%
Absorption correction	Semi-empirical from equivalents
Max. and min. transmission	0.9361 and 0.8847
Refinement method	Full-matrix least-squares on F^2
Data/restraints / parameters	1,435/2/146
Goodness-of-fit on F^2	1.071
Final R indices [$I > 2\sigma(I)$]	$R_1 = 0.0385$, $wR_2 = 0.0797$
R indices (all data)	$R_1 = 0.0527$, $wR_2 = 0.0842$
Absolute structure parameter	0.06(11)
Extinction coefficient	0.0020(10)
$\rho_{min/max}$ (e Å^{-3})	0.191 and –0.173

Similarly, carefully compared with the FI-IR spectra of ligand HL^2, the bands of N–H of 3,207 cm^{-1} disappear, and new bands of 1,616 cm^{-1} and 1,524-1,501 cm^{-1} appears, indicating the enolized and deprotonated $^-$O–C=N– involves in coordination. Additionally, the new bands of 781-771 cm^{-1}, 608-519 cm^{-1} and 474-419 cm^{-1} also show further the formations of S–M, O–M and N–M bonds, respectively. Moreover, for complexes of rare earth metal ions, new bands of 1,242-1,238 cm^{-1} and 1,057-1,045 cm^{-1} are due to the asymmetric and symmetric stretches of coordinated nitrate group, respectively[34,35]. Furthemore, for Sc^{3+} complex, the bands of 941 cm^{-1} and 656 cm^{-1} are due to stretches of ρ_r and ρ_w of coordinated H_2O molecules, respectively[36,37]. Combined with the data of molar conductivities, elemental analysis, FT-IR and ESI-MS (m/z^+), it suggests that HL^2 also exhibits a tridentate and anion ligand and uses oxygen anion, nitrogen atom and sulfur atom to coordinate with metal ions. The suggested chemical structures of Co^{2+}, Cu^{2+} and Zn^{2+} complexes derived from HL^2 are presented in Figure 6b, the suggested chemical structures of Sc^{3+} complex derived from HL^2 are presented in Figure 6c, and the suggested chemical structures of Pr^{3+} and Dy^{3+}complexes derived from HL^2 are presented in Figure 6d.

DNA Binding Properties

In case of lack of crystal structure data, hydrodynamic measurement is considered to be the most unambiguous and critical standard for binding modes of DNA and compound in solution, because viscosity is related to the length L^3 of rod-like DNA[25,38]. With the increasing of the $C_{compound}/C_{DNA\ (bps)}$, the relative viscosities of CT-DNA increase persistently, as shown in Figure 2 (the effect resulted from solvent was not corrected). This indicates that intercalation exists between the present compound and CT-DNA helix, in which the intercalating agent causes unwinding and extension of CT-DNA, and thus improves relative viscosity of CT-DNA[26,39,40].

As listed in Table IV, UV-Vis spectra of ligand H_2L^1 presents two bands of 270 nm (ε = 0.7757×10^4 L mol^{-1} cm^{-1}) and 324 nm (ε = 1.926×10^4 L mol^{-1} cm^{-1}), while UV-Vis spectra of its metal complexes presents two bands of 254-262 nm (ε = 1.324-1.780×10^4 L mol^{-1} cm^{-1}) and 356-370 nm (ε = 0.6825-1.379×10^4 L

Table III. Comparison of the measured bond length of ligand HL2 with the normal one.

Measured bond length (Å)		Normal bond length (Å)[32]	
C1–O1	1.218 (4) (C···)C=O	C–O	1.30-1.39
		1.19-1.23	
C1–N1	1.337 (4)	C–N	1.47-1.50
C7–N2	1.263 (5)	C = N (conjugate)	1.34-1.38
N1–N2	1.385 (4)	N = N	1.22-1.30

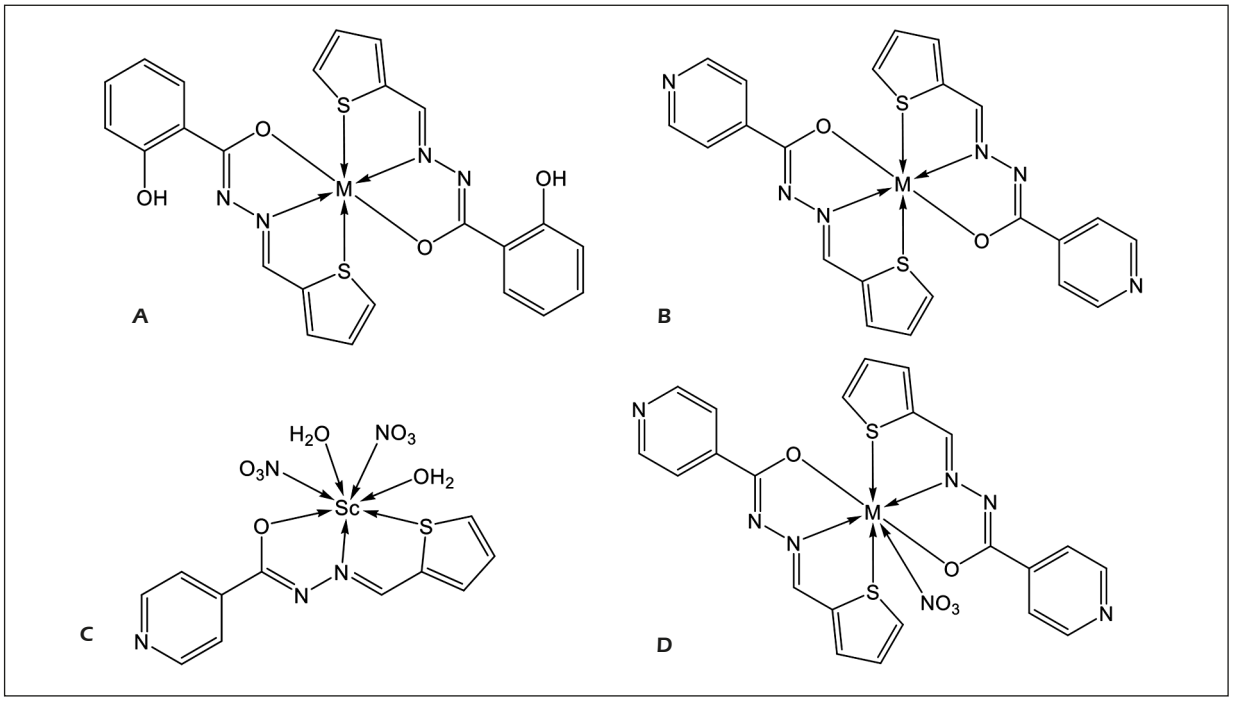

Figure 6. Suggested chemical structures of complexes derived from H2L1 and HL2. **A**, M = Cu2+, Ni2+ and Co2+; **B**, M = Co2+, Cu2+ and Zn2+; **C**, Sc3+ complex; **D**, M = Pr3+ and Dy3+.

mol^{-1} cm^{-1}), which are due to π-π* transition and charge transfer of $L \rightarrow M^{n+}$, respectively[36,37]. With successive addition of CT-DNA (4.0-40.0 μmol L^{-1}), the UV-Vis band of 270 nm of ligand H_2L^1 show successive hyperchromicities with the hyperchromicity rate of 124.9% and 14 nm blue shifts, while the band of 322 nm show a hyperchromicity first (exceeding the absorption value of the H_2L^1 itself) and then successive hypochromicities with the hypochromicity rate of 9.73% and no shift. With successive addition of CT-DNA (4.0-40.0 μmol L^{-1}), the UV-Vis band of 254 nm of complex $[Co(HL^1)_2]$ show successive hyperchromicities with the hyperchromicity rate of 23.93% and 5 nm red shifts, while the band of 363 nm show successive hypochromicities with the hypochromicity rate of 46.15% and no shift; the UV-Vis band of 254 nm of complex $[Ni(HL^1)_2]$ show successive hyperchromicities with the hyperchromicity rate of 59.71% and 5 nm red shifts, while the band of 356 nm show successive hypochromicities with the hypochromicity rate of 27.64% and 8 nm blue shifts; the UV-Vis band of 262 nm of complex $[Cu(HL^1)_2]$ show a successive hyperchromicity with the hyperchromicity rate of 68.42% and 2 nm blue shifts, while the band of λ_{max} at 370 nm of $[Cu(HL^1)_2]$ show a hypochromicity first and then successive hyperchromicities – exceeding the absorption value of the $[Cu(HL^1)_2]$ itself – with the hyperchromicity rate of 68.42% and no shift.

As shown in Figure 3, there are two UV-Vis bands of 273 nm ($\varepsilon = 1.048\times10^4$ L mol^{-1} cm^{-1}) and 324 nm ($\varepsilon = 2.004\times10^4$ L mol^{-1} cm^{-1}) for HL^2, and there are two bands of 256-283 nm (ε = 0.6627-1.114×10^4 L mol^{-1} cm^{-1}) and 321-366 nm (ε = 0.5373-2.004×10^4 L mol^{-1} cm^{-1}) for its metal complexes, which are also due to π-π* transition and charge transfer of $L \rightarrow M^{n+}$, respectively[36,37]. With successive addition of CT-DNA (4.0-40.0 μmol L^{-1}), the UV-Vis band of 273 nm of HL^2 show successive hyperchromicities with the hyperchromicity rate of 75.76% and 9 nm blue shifts, while the band of 324 nm show a hyperchromicity first (exceeding the absorption value of the HL^2 itself), and then successive hypochromicities with the hypochromicity rate of 6.54% and no shift. With successive addition of CT-DNA (4.0-40.0 μmol L^{-1}), all of the UV-Vis bands of 256-283 nm of complexes show successive hyperchromicities with the hyperchromicity rate of 77.90-167.4% and 2-25 nm blue shifts; while the bands of 366 nm and 349 nm of both complexes $[Co(HL^2)_2]$ and $[Cu(HL^2)_2]$ show successive hypochromicities, with the hypochromicity rate of

Table IV. The UV-vis spectra values, hypochromicity or hyperchromicity and shifts of λ_{max}, K_b for investigated compounds in the presence of CT-DNA.

Compound	π–π* conjugated aromatic ring		π–π* C=N–N=C and (L→M^{n+})		K_b (×10^4, L mol^{-1}) (R^2)
	λ_{max} (ε×10^4 L mol^{-1} cm^{-1})	Hypochromicity or hyperchromicity (λ_{max} shifts)	λ_{max} (ε×10^4 L mol^{-1} cm^{-1})	Hypochromicity or hyperchromicity (λ_{max} shifts)	
H_2L^1	270 (0.7757)	124.9% (hyperchromicity, 14 nm blue)	322 (1.926)	9.73% (hypochromicity, no shift) (hyperchromicity first and then hypochromicity)	17.60±7.57 (0.7720)
$[Co(HL^1)_2]$	254 (1.650)	23.93% (hyperchromicity, 5 nm red)	363 (1.379)	46.15% (hypochromicity, no shift)	3.277±0.40 (0.9747)
$[Ni(HL^1)_2]$	254 (1.324)	59.71% (hyperchromicity, 5 nm red)	356 (1.335)	27.64% (hypochromicity, 8 nm blue)	51.25±4.03 (0.8470)
$[Cu(HL^1)_2]$	262 (1.780)	68.42% (hyperchromicity, 2 nm blue)	370 (0.6825)	68.42% (hyperchromicity, no shift) (hypochromicity first and then hyperchromicity)	21.31±6.42 (0.8972)
HL^2	273 (1.048)	75.76% (hyperchromicity, 9 nm blue)	324 (2.004)	6.54% (hypochromicity, no shift) (hyperchromicity, over, hypochromicity, no shift)	17.22±5.89 (0.9549)
$[Co(L^2)_2]$	283 (1.114)	77.90% (hyperchromicity, 25 nm blue)	366 (1.003)	26.63% (hypochromicity, no shift)	7.680±0.40 (0.9792)
$[Cu(L^2)_2]$	256 (0.6641)	167.4% (hyperchromicity, 14 nm blue)	349 (0.5373)	24.75% (hypochromicity, no shift)	67.95±4.03 (0.8668)
$[Zn(L^2)_2]$	269 (0.8854)	104.9% (hyperchromicity, 17 nm blue)	321 (1.940)	10.62% (hyperchromicity, no shift)	4.231±0.49 (0.6051)
$[ScL^2(NO_3)_2(H_2O)_2]$	263 (1.035)	94.66% (hyperchromicity, 2 nm blue)	324 (2.232)	5.09% (hypochromicity, no shift)	31.51±4.95 (0.8017)
$[Pr(L^2)_2(NO_3)]$	267 (0.6627)	173.3% (hyperchromicity, 9 nm blue)	322 (1.556)	3.12% (hyperchromicity, no shift) (hyperchromicity, hypochromicity)	35.21±4.03 (0.7780)
$[Dy(L^2)_2(NO_3)]$	268 (0.6749)	154.5% (hyperchromicity, 7 nm blue)	322 (1.443)	6.00% (hyperchromicity, no shift) (hyperchromicity, hypochromicity)	36.55±4.03 (0.9664)

26.63% and 24.75% and no shifts, respectively. The bands of 321 nm of $[Zn(HL^2)_2]$ show successive hyperchromicities with the hyperchromicity rate of 10.62% and no shift; the band of 324 nm of $[ScL^2(NO_3)_2(H_2O)_2]$ show successive hypochromicities with the hypochromicity rate of 5.09% and no shift; the bands of 322 nm of both complexes $[Pr(L^2)_2(NO_3)]$ and $[Dy(L^2)_2(NO_3)]$ show a successive hyperchromicities first and then successive hypochromicities with the hyperchromicity rate of 3.12% and 6.00% and no shift, respectively.

Many metal complexes have absorption bands, and their interaction modes can be judged according to the changes of UV-Vis absorption bands before and after their interaction with DNA[41]. For the characteristic absorption bands of molecules, such as metal complexes, if the molecule has insertion with DNA, the position of absorption peak of electron absorption spectrum of molecule will shift red, and the intensity will decrease[42]. The reason for this phenomenon is that the insertion ligand and DNA base pair can produce π electron accumulation, and π*

empty orbit of acting ligand is coupled with π electron orbit of bases, which reduces the energy level, resulting in energy reduction of π-π* transition and achromatic effect, red shifts. Studies[41] have shown that the bonding between small molecules and DNA often induces many biological effects. When heterocyclic complexes interact with DNA, planar aromatic ligands are partially embedded between adjacent base pairs of DNA. This insertion is an important mode of binding between drug molecules and DNA, and metal inserters are very useful probes for this mode of binding[41]. Some metal insertion agents are selected by shape, such as Δ-[Rh(DP-B)2phi]$^{3+}$ (phi = phenanthrene-quinone diimide), while some rely on hydrogen bond and van der Waals force to act on the large groove region of DNA, and most complexes derived from rhodium with amine ligands belong to this kind. A series of derivatives with guanidine groups based on $Rh(phen)_2phi^{3+}$ are also a kind of metal intercalators with high selectivity and good binding because they have both shape selection, hydrogen bond and van der Waals force[43]. If complex has electrostatic or grooving interaction mode with DNA, its UV-Vis band will not have a red shift (or a small and negligible red shift), and the hypochromicity effect is not obvious[42]. Zhou et al[44] studied the interaction of complex $Co(bpy)_3^{3+}$-6-MP with DNA and found that the UV-vis absorption of complex decreases but there is no red shift, due to electrostatic interaction. Liu et al[45] found after combined with DNA in a groove pattern, the UV-Vis absorption of $[Cu_4(dmapox)_2(SCN)_4(CH_3CH_2OH)_2]_n \cdot 2nCH_3CH_2OH$ also reduced without red shift. Senthil Kumar and Arunachalam[46] studied the interaction between cis-$[Co(bpy)^2(BPEI)Cl]Cl_2 \cdot 4H_2O$ and CT-DNA, and found that, with the addition of DNA, UV-Vis absorption of complex showed an obvious hyperchromicity effect, and inferred that there was a hydrogen bond between them. The interaction mode between compound and CT-DNA will also change with the change of conditions. Zhang et al[47] synthesized and characterized $[Cu_2(DL\text{-}ASP)(phen)_3]SO_4 \cdot 4H_2O$, and studied the interaction mode. When complex begins to interact with DNA, UV-Vis absorption decreases significantly and red shifts. However, in case of gradual increase of DNA concentration, UV-Vis absorption of the complex begins to increase after the UV-Vis absorption is reduced to a certain extent, and the UV-Vis absorption enhancement is much greater than the original UV-Vis absorption of the complex. It shows that, when the DNA concentration is low, the complex and DNA are mainly inserted, but when the DNA concentration is high, there is a hydrogen bond between them, so that UV-Vis absorption of complex shows a phenomenon of first subtraction and then enhancement.

EB+DNA+compound system (EB as classical intercalative agent) has been introduced to further elucidate the interaction pattern between compounds and DNA. As shown in Figure 4, the classical DNA intercalator EB (10.0 μmol L^{-1}) shows a UV-Vis band of 285 nm. After DNA (45.0 μmol L^{-1}) is added, the EB+DNA system shows a UV-Vis band of λ_{max} at 263 nm with 22 nm blue shifts, which indicates that EB is in a more hydrophobic environment after inserting base pairs of DNA. Upon successive addition of HL^2 (4.0-40.0 μmol L^{-1}) to this EB+DNA system, the UV-Vis band of 271 nm and band of 322 nm shows successive hyperchromicities, which is slightly different from the UV-Vis bands of HL^2 itself of 273 nm and 324 nm, indicating that EB is partly replaced by HL^2 from EB-DNA system. Similarly, upon successive addition of $[Co(HL^2)_2]$ (4.0-40.0 μmol L^{-1}) to the EB+DNA system, the UV-Vis band of 282 nm and band of 356 nm shows successive hyperchromicities, which is also slight different from the UV-Vis bands of $[Co(HL^2)_2]$ itself of 283 nm and 366 nm, indicating that EB is partly replaced by $[Co(HL^2)_2]$ from EB-DNA system, too. Combined with the viscosity analysis results, it infers that all the ligands and complexes can interact with CT-DNA mainly by hydrogen bond and insertion; however, the groove pattern may not be excluded.

The binding constants (K_b = 3.277-67.95 × 10^4 L mol^{-1}) of CT-DNA and the investigated compounds calculated are listed in Table IV. In comparison with EB interacting with DNA ($K_{b\,(EB-DNA)}$ = 3.068 × 10^4 L mol^{-1}) at the same experimental conditions[29,48], all the ligands and their complexes show strongly interacting abilities with DNA. However, complexes $[Co(HL^1)_2]$, $[Co(HL^2)_2]$ and $[Zn(HL^2)_2]$ show little weaker binding abilities than their ligands, while the other complexes show stronger binding abilities than their ligands. Especially, complex $[Cu(HL^2)_2]$ show stronger binding ability than the others. Generally, the rare-earth metal complexes show strongly interacting abilities with DNA. However, the present complexes show weaker or equivalent interacting abilities with DNA than complexes derived from 8-hydroxyquinoline-2-carboxaldehyde-hy-

drazone (K_b = 1.422-285.3 × 10^5 L mol^{-1})[29,30,49-59], 8-hydroxyquinoline-7-carboxaldehyde-hydrazone (K_b = 2.938-26.13 × 10^5 L mol^{-1})[48,60], 3-carbaldehyde-chromone-isonicotinyl-hydrazone, 1-phenyl-3-methyl-4-formyl-2-pyrazolin-5-one (PMFP)-isonicotinyl-hydrazone and PMFP-4-aminophenazone (K_b = 2.44-7.6 × 10^5 L mol^{-1})[61-63].

$[Ni(HL^1)_2]$ or $[Cu(HL^1)_2]$ Assay

As shown in Table I (*$p < 0.05$) and Figure 5, HeLa cell shows lower viabilities in the presence of $[Ni(HL^1)_2]$ or $[Cu(HL^1)_2]$ compared to both ligands and the other complexes, that is, both of $[Ni(HL^1)_2]$ and $[Cu(HL^1)_2]$ present higher viability inhibitions for HeLa cells. By fitting mathematical formula with scatter plot of cell viability ratio *vs.* molar concentration of compound, the relationship between cell viability ratio (y) and molar concentration (x) presents an exponential function of $y = 0.8844e^{-0.219x}$ (R^2 = 0.8734) for $[Ni(HL^1)_2]$ and $y = 0.9363e^{-0.279x}$ (R^2 = 0.9253) for $[Cu(HL^1)_2]$, then the values of LC_{50} (half lethal concentration) calculated according to the relationship are 2.6 μmol L^{-1} and 2.2 μmol L^{-1} for $[Ni(HL^1)_2]$ and $[Cu(HL^1)_2]$, respectively.

Conclusions

A series of metal complexes derived from (*E*)-2-hydroxy-*N'*-((thiophen-2-yl)methylene)benzohydrazone and (*E*)-*N'*-((thiophen-2-yl)methylene) isonicotinylhydrazone were synthesized and the structures were characterized. Ligands and their metal complexes could interact strongly with CT-DNA through the main modes of hydrogen bond and intercalation with the binding constants at 10^4-10^5 L mol^{-1} compared to EB; however, the groove pattern would not be excluded. The coexistence of multiple binding modes may be a common form of drug binding to DNA. Moreover, $[Ni(HL^1)_2]$ and $[Cu(HL^1)_2]$ presented higher abilities than the ligand binding to DNA, and $[Cu(L^2)_2]$, $[ScL^2(NO_3)_2(H_2O)_2]$, $[Pr(L^2)_2(NO_3)]$ and $[Dy(L^2)_2(NO_3)]$ showed higher abilities than the ligand. Furthermore, HeLa showed lower viabilities in the present of $[Ni(HL^1)_2]$ and $[Cu(HL^1)_2]$ (*$p < 0.05$), compared to the ligands and other compounds, with the LC_{50} at the concentration of 2.6 μmol L^{-1} and 2.2 μmol L^{-1}, respectively. These compounds would be promising for drugs in the clinical treatment of cancer, which should be further studied.

Conflict of Interest
The Authors declare that they have no conflict of interests.

Funding
This study was supported from the Natural Science Foundation of Gansu (No. 21JR7RM187) and Project of Science and Technology Department of Gansu (No. 21JR1RM336).

Authors' Contribution
Y.-C. Liu: Planning, designing, data collection, literature survey, interpretation of the results, writing manuscript, conception of the work, English editing. X. Zhang and B.-D. Wang: Data collection and statistical analysis of cell viability assay. J.-Y. Wang, G.-P. Zhao, C.-X. Bai and H. Chen: Data collection and analysis of DNA binding properties and syntheses of ligands and metal complexes. J. Luo, S.-Y. Wang, Z.-X. Liang, Y.-Y. Li and R.-X. Lei: Conception of the work and interpretation of the results.

ORCID ID
Y.-C. Liu: 0000-0002-3243-7384.

Ethics Approval
This study does not involve animal organism testing, therefore ethics approval is not required.

References

1) Cocco MT, Congiu C, Lilliu V, Onnis V. Synthesis and in vitro antitumoral activity of new hydrazinopyrimidine-5-carbonitrile derivatives. Bioorg Med Chem 2006; 14: 366-372.
2) Terzioglu N, Gürsoy A. Synthesis and anticancer evaluation of some new hydrazone derivatives of 2,6-dimethylimidazo[2,1-b]-[1,3,4]thiadiazole-5-carbohydrazide. Eur J Med Chem 2003; 38: 781-786.
3) Easmon J, Puerstinger G, Roth T, Fiebig HH, Jenny M, Jaeger W, Heinisch G, Hofmann J. 2-benzoxazolyl and 2-benzimidazolyl hydrazones derived from 2-acetylpyridine: a novel class of antitumor agents. Int J Cancer 2001; 94: 89-96.
4) Vicini P, Zani F, Cozzini P, Doytchinova I. Hydrazones of 1,2-benzisothiazole hydrazides: synthesis, antimicrobial activity and QSAR investigations. Eur J Med Chem 2002; 37: 553-564.
5) Isloor AM, Kalluraya B, Pai KS. Synthesis, characterization and biological activities of some new benzo[b]thiophene derivatives. Eur J Med Chem 2010; 45: 825-830.
6) Anti-Tuberculosis Association of China. Chemotherapeutic guidelines for drug resistant tuberculosis (short version 2019, in Chinese). Chin J Antituberc 2019: 41: 1025-1073.

7) Tian L, Zhou W, Huang X, Wu XW, Zhang HY, Lu ZH, Zhang SY. Analysis of gene mutation characteristics of isoniazid-resistant Mycobacterium tuberculosis in China. Chin J Antituberc 2022; 44: 354-361.
8) Liu BG, Yuan XL, He DD, Hu GZ, Miao MS, Xu EP. Research progress on the oxazolidinone drug linezolid resistance. Eur Rev Med Pharmacol Sci 2020; 24: 9274-9281.
9) Liu HR, Zhao J. effect and mechanism of miR-217 on drug resistance, invasion and metastasis of ovarian cancers through a regulatory axis of CUL4B gene silencing/inhibited Wnt/β-catenin signaling pathway activation. Eur Rev Med Pharmacol Sci 2021; 25: 94-107.
10) Fouad R. Synthesis and characterization of lanthanide complexes as potential therapeutic agents. J Coord Chem 2020; 73: 2015-2028.
11) Teo RD, Termini J, Gray HB. Lanthanides: Applications in Cancer Diagnosis and Therapy Miniperspective. J Med Chem 2016; 59: 6012-6024.
12) Reji TFAF, Pearl AJ, Rosy BA. Synthesis, characterization, cytotoxicity, DNA cleavage and antimicrobial activity of homodinuclear lanthanide complexes of phenylthioacetic acid. J Rare Earths 2013; 31: 1009-1016.
13) Shakir M, Abbasi A, Faraz M, Sherwani A. Synthesis, characterization and cytotoxicity of rare earth metal ion complexes of N,N′-bis-(2-thiophenecarboxaldimine)-3,3′-diaminobenzidene, Schiff base ligand. J Mol Struc 2015; 1102: 108-116.
14) Song P, Fang Z, Tong L. Effects of metal chelates on a novel oligomeric intumescent flameretardant system for polypropylene. J Anal Appl Pyrolysis 2008; 82: 286-291.
15) Hodnett EM, Dunn WJ. Cobalt derivatives of Schiff bases of aliphatic amines as antitumor agents. J Med Chem; 1972, 15: 339.
16) Hodnett EM, Mooney PD. Antitumor activities of some Schiff bases. J Med Chem 1970; 13: 786.
17) Zeng YB, Yang N, Liu WS, Tang N. Synthesis, characterization and DNA-binding properties of La(III) complex of chrysin. J Inorg Biochem 2003; 97: 258-264.
18) Pyle AM, Morii T, Barton JK. Probing microstructures in double-helical DNA with chiral metal complexes: recognition of changes in base-pair propeller twisting in solution. J Am Chem Soc 1990; 112: 9432-9434.
19) Barton JK, Goldberg JM, Kumar CV, Turro NJ. Binding modes and base specifificity of tris(phenanthroline) ruthenium(II) enantiomers with nucleic acids: tuning the stereoselectivity. J Am Chem Soc 1986; 108: 2081-2088.
20) Mahadevan S, Palaniandavar M. Spectroscopic and voltammetric studies of copper(II) complexes of bis(pyrid-2-yl)-di/trithia ligands bound to calf thymus DNA. Inorg Chim Acta 1997; 254: 291-302.
21) Lippard SJ. Platinum complexes: probes of polynucleotide structure and antitumor drugs. Acc Chem Res 1978; 11: 211-217.
22) Hecht SM. The chemistry of activated bleomycin. Acc Chem Res 1986; 19: 383-391.
23) El-Shafiy HF, Saif M, Mashaly MM, Halim SA, Eid MF, Nabeel AI, Fouad R. New nano-complexes of Zn(II), Cu(II), Ni(II) and Co(II) ions; spectroscopy, thermal, structural analysis, DFT calculations and antimicrobial activity application. J Mol Struc 2017; 1147: 452-461.
24) Zsila F, Bikádi Z, Simonyi M. Circular dichroism spectroscopic studies reveal pH dependent binding of curcumin in the minor groove of natural and synthetic nucleic acids. Org Biomol Chem 2004; 2: 2902-2910.
25) Suh D, Chaires JB. Criteria for the mode of binding of DNA binding agents. Bioorgan. Med Chem 1995; 3: 723-728.
26) Satyanarayana S, Dabrowiak JC, Chaires JB. Neither Δ-nor Λ-Tris(phenanthroline)ruthenium(II) Binds to DNA by Classical Intercalation. Biochemistry 1992; 31: 9319-9324.
27) Wolfe A, Shimer GH, Jr Meehan T. Polycyclic aromatic hydrocarbons physically intercalate into duplex regions of denatured DNA. Biochemistry 1987; 26: 6392-6396.
28) Xi PX, Xu ZH, Liu XH, Cheng FJ, Zeng ZZ. Synthesis, characterization and DNA-binding studies of 1-cyclohexyl-3-tosylurea and its Ni(II), and Cd(II) complexes. Spectrochim Acta A Mol Biomol Spectrosc 2008; 71: 523-528.
29) Liu Y, Yang Z, Zhang K, Wu Y, Zhu J, Zhou T. Crystal Structures, Antioxidation, and DNA Binding Properties of SmIII Complexes. Aust J Chem 2011; 64: 345-354.
30) Liu YC, Li YY., Qi HL, Hu HS, Zhang KJ, Lei RX, Liu JN, Zheng XD. DNA Binding Properties of Sc(III) Complexes Derived from Rare-earth(III) Ions and Semicarbazone of 8-hydroxyquinoline-2-carbaldehyde. Russ J Coord Chem 2019; 45: 446-456.
31) Sheldrick GM. Phase annealing in SHELX-90: direct methods for larger structures. Acta Crystallogr. A 1990; 46: 467-473.
32) Chen XM, Cai JW. Single-Crystal Structural Analysis. Principles and Practices M], Beijing: Science Press, 2003: 114.
33) Geary WJ. The use of conductivity measurements in organic solvents for the characterisation of coordination compounds. Coord Chem Rev 1971; 7: 81-122.
34) Saif M, Mashaly MM, Eid MF, Fouad R. Synthesis and thermal studies of tetraazamacrocylic ligand and its transition metal complexes. DNA binding affifinity of copper complex. Spectrochim Acta Part A 2011; 79: 1849-1855.
35) Saif M, Mashaly MM, Eid MF, Fouad R. Synthesis, characterization and thermal studies of binary and/or mixed ligand complexes of Cd(II),

Cu(II), Ni(II) and Co(III) based on 2-(Hydroxybenzylidene) thiosemicarbazone: DNA binding affifinity of binary Cu(II) complex. Spectrochim Acta A Chem 2012; 92: 347-356.

36) Ismailt TMA. Mononuclear and binuclear Co(II), Ni(II), Cu(II), Zn(II) and Cd(II) complexes of Schiff-base ligands derived from 7-formyl-8-hydroxyquinoline and diaminonaphthalenes. J Coord Chem 2005; 58: 141-151.

37) Moawad MM, Hanna WG. Structural and antimicrobial studies of some divalent transition metal complexes with some new symmetrical bis(7-formylanil substituented-sulfoxine) Schiff base ligands. J Coord Chem 2002; 55: 439-457.

38) Sigman DS, Mazumder A, Perrin DM. Chemical Nucleases. Chem Rev 1993; 93: 2295-2316.

39) Palchaudhuri R, Hergenrother PJ. DNA as a target for anticancer compounds: methods to determine the mode of binding and the mechanism of action. Curr Opin Biotech 2007; 18: 497-503.

40) Wang B-d, Yang Z-y, Crewdson P, Wang D-q. Synthesis, crystal structure and DNA-binding study on the Ln(III) complex of 6-hydroxychromone-3-carbaldehyde benzoyl hydrazone.J Inorg Biochem 2007; 101: 1492-1504.

41) Gao T, Zhang WJ, Wang F, Zhang HB, Zhang W. Application of UV Spectra in the Interaction of DNA and Metal Complexes. Guangzhou Chemical Industry (in Chinese) 2010; 38: 23-25.

42) Breslow R, Overman IE. "Artificial enzyme" combining a metal catalytic group and a hydrophobic binding cavity. J Am Chem Soc 1970; 92: 1075-1077.

43) Zhou J, Yuan G. Recent Progress in DNA Recognition Molecules. Chinese Journal of Organic Chemistry (in Chinese) 2003; 23: 526-541.

44) Zhou CF, Du XS, Li H. Studies of interactions among cobalt(III) poly-pyridyl complexes, 6-memaptopurine and DNA. Bioelectrochemistry 2006; 71: 189-194.

45) Liu ZQ, Jiang M, Li YT. One-dimensional copper(II) polymer with bridging-μ-trans-oxamidate and thiocyanato ligands: synthesis, crystal structure and DNA binding studies. Inorg Chim Acta 2009; 362: 1253-1259.

46) Senthil Kumar R, Arunachalam S. Synthesis, characterization and DNA binding studies of a polymer-cobalt(III) complex containing the 2,2'-bipyridyl ligand. Polyhedron 2006; 25: 3113-3117.

47) Zhang F, Zhang QQ, Wang WG, Wang XL. Synthesis and DNA binding studies by spectroscopic and PARAFAC methods of a tomary copper (ii) complex. J Photochem Photobiol A: Chemistry 2006; 184: 241-249.

48) Liu Y, Zhang K, Lei R, Liu J, Zhou T, Yang ZY. DNA-binding and anti-oxidationproperties of binuclear lanthanide(III) complexes of 8-hydroxyquinoline-7-carbaldehyde-(isonicotinyl)hydrazone. J Coord Chem 2012; 65: 2041-2054.

49) Liu YC, Li YY, Qi HL, Hu HS, Zhang KJ, Lei RX, Liu JN. Crystal Structures and DNA Binding Properties of Yttrium (III) Complexes Derived from 8-Hydroxyquinoline-2-carboxaldehydearoylhydrazones. Russ J Coord Chem (in Russian) 2017; 43: 434-443.

50) Liu Y, Li Y, Qi H, Hu H, Lei R, Liu J. DNA Binding Properties of ScandiumIII Complexes Derived from Three 8-Hydroxyquinoline-2-carboxaldehyde-aroylhydrazones M]. Biotechnol Med Sci 2016: 392-399.

51) Lei RX, Ma DP, Zhang XW, Liu YC, Zheng X, Liu JN, Yang ZY. Binuclear lanthanide complexes derived from aroylhydrazineswith 8-hydroxyquinoline-2-carboxyaldehyde and a series of DNA intercalators M]. In Medicine Sciences and Bioengineering (ICMSB 2014) (Ed. Wang) 2015: 783-791.

52) Liu YC, Li YY, Qi HL, Zhang KJ, Lei RX, Liu JN. Crystal structures and DNA-binding properties of PrIII complexes derived from 8-hydroxyquinoline-2-carboxaldehyde and three aroylhydrazines. J Coord Chem 2014; 67: 3689-3703.

53) Liu Y, Jiang X, Yang Z, Zheng X, Liu J, Zhou T. Fluorescent and Ultraviolet–Visible Spectroscopy Studies on the Antioxidation and DNA Binding Properties of Binuclear Tb(III) Complexes. Appl Spectrosc 2010; 64: 980-985.

54) Liu Y, Yang ZY. Antioxidation and DNA-binding properties of binuclear Er(III) complexes with Schiff-base ligands derived from 8-hydroxyquinoline-2-carboxaldehyde and four aroylhydrazines. J Biochem 2010; 147: 381-391.

55) Liu YC, Yang ZY. Crystal structures, antioxidation and DNA binding properties of Eu(III) complexes with Schiff-base ligands derived from 8-hydroxyquinoline-2-carboxyaldehyde and three aroylhydrazines. J Inorg Biochem 2009; 103: 1014-1022.

56) Liu YC, Yang ZY. Crystal structure, antioxidation and DNA binding properties of binuclear Ho(III) complexes of Schiff-base ligands derived from 8-hydroxyquinoline-2-carboxyaldehyde and four aroylhydrazines. J Organomet Chem 2009; 694: 3091-3101.

57) Liu YC, Yang ZY. Crystal structures, antioxidation and DNA binding properties of Dy(III) complexes with Schiff-base ligands derived from 8-hydroxyquinoline-2-carboxaldehyde and four aroylhydrazines. Eur J Med Chem 2009; 44: 5080-5089.

58) Liu YC, Yang ZY. Crystal structures, antioxidation and DNA binding properties of Yb(III) complexes with Schiff-base ligands derived from 8-hydroxyquinoline-2-carbaldehyde and four aroylhydrazines. Biometals 2009; 22: 733-751.

59) Liu YC, Yang ZY. Antioxidation and DNA binding properties of binuclear Nd(III) complexes with Schiff-base ligands derived from 8-hydroxyquinoline-2-carboxyaldehyde and four aroylhydrazides. Inorg Chem Commun 2009; 12: 704-706.

60) Liu Y, Zhang K, Wu Y, Zhao J, Liu J. Antioxidation and DNA-Binding Properties of Binuclear Lanthanide(III) Complexes with a Schiff Base Ligand Derived from 8-Hydroxyquinoline-7-carboxaldehyde and Benzoylhydrazine. Chem Biodivers 2012; 9: 1533-1544.

61) Li Y, Yang ZY. DNA-binding properties and antioxidant activity of lanthanide complexes with the Schiff base derived from 3-carbaldehyde chromone and isonicotinyl hydrazine. J Coord Chem 2010; 63: 1960-1968.

62) Wang M, Yang Z, Li Y, Li H. Lanthanide complex of 1-phenyl-3-methyl-5-hydroxypyrazole-4-carbaldehyde-(isonicotinoyl)hydrazone: crystal structure and DNA-binding properties. J Coord Chem 2011; 64: 2974-2983.

63) Wang MF, Yang ZY, Liu ZC, Li Y, Li TR, Yan MH, Cheng XY. Synthesis and crystal structure of a Schiff base derived from two similar pyrazolone rings and its rare earth complexes: DNA-binding and antioxidant activity. J Coord Chem 2012; 65: 3805-3820.